Monitoring tumor cell death in murine tumor models using deuterium magnetic resonance spectroscopy and spectroscopic imaging

Friederike Hesse[1†], Vencel Somai[1,2†], Felix Kreis[3], Flaviu Bulat[1, 4], Alan J. Wright[1], Kevin M. Brindle[1,5*]

[1]Cancer Research UK Cambridge Institute, University of Cambridge, Li Ka Shing Centre, Robinson Way, Cambridge, United Kingdom.

[2]Department of Radiology, University of Cambridge, School of Clinical Medicine Box 218, Cambridge Biomedical Campus

[3]Department Information Technology and Electrical Engineering, ETH Zurich, Rämistrasse 101, Zürich, ZH, Switzerland

[4]Department of Chemistry, University of Cambridge, Lensfield Road, Cambridge, United Kingdom

[5]Department of Biochemistry, University of Cambridge, Tennis Court Road, Cambridge, United Kingdom.

*Correspondence to: K.M. Brindle, D. Phil., Cancer Research UK Cambridge Institute, Li Ka Shing Centre, Robinson Way, Cambridge, CB2 0RE, UK; E-mail: kmb1001@cam.ac.uk

†These authors contributed equally to this work.

Classification: Biological Sciences; Applied Biological Sciences

Keywords: cell death, tumor, MRI, deuterium

Abstract

^{2}H magnetic resonance spectroscopic imaging has been shown recently to be a viable technique for metabolic imaging in the clinic. We show here that ^{2}H MR spectroscopy and spectroscopic imaging measurements of [2,3-$^{2}H_2$]malate production from [2,3-$^{2}H_2$]fumarate can be used to detect tumor cell death in vivo via the production of labeled malate. Production of [2,3-$^{2}H_2$]malate, following injection of [2,3-$^{2}H_2$]fumarate (1 g/kg) into tumor-bearing mice, was measured in a murine lymphoma (EL4) treated with etoposide, and in human breast (MDA-MB-231) and colorectal (Colo205) xenografts treated with a TRAILR2 agonist, using surface-coil localized ^{2}H MR spectroscopy at 7 T. Malate production was also imaged in EL4 tumors using a fast ^{2}H chemical shift imaging sequence. The malate/fumarate ratio increased from 0.016 ± 0.02 to 0.16 ± 0.14 in EL4 tumors 48 h after drug treatment (P=0.0024, n=3), and from 0.019 ± 0.03 to 0.25 ± 0.23 in MDA-MB-231 tumors (P = 0.0001, n=5) and from 0.016 ± 0.04 to 0.28 ± 0.26 in Colo205 tumors (P = 0.0002, n=5) 24 h after drug treatment. These increases were correlated with increased levels of cell death measured in excised tumor sections obtained immediately after imaging. ^{2}H MR measurements of [2,3-$^{2}H_2$]malate production from [2,3-$^{2}H_2$]fumarate provides a potentially less expensive and more sensitive method for detecting cell death in vivo than ^{13}C MR measurements of hyperpolarized [1,4-$^{13}C_2$]fumarate metabolism, which have been used previously for this purpose.

Significance statement

There is an unmet clinical need for sensitive methods for detecting cell death in vivo, for example in disease and following tumor treatment. We show here that deuterium magnetic resonance measurements at 7 T of labeled malate production from injected ^{2}H-labelled fumarate provides a sensitive method for detecting tumor cell death in vivo following treatment. Malate production was relatively slow in viable cells but was markedly increased in necrotic tissue.

Introduction

Currently the response of solid tumors to treatment is assessed mainly on the basis of changes in tumor size (Response Evaluation Criteria in Solid Tumors (RECIST) (1). However, changes in size may take weeks to appear after the initiation of treatment, and in some cases may not appear at all, for example in the case of treatments that inhibit tumor growth but do not result in tumor regression (2, 3). Changes in metabolism can give an earlier indication of treatment response, for example assessment of glycolytic activity using PET measurements of 2-[^{18}F]-fluoro-2-deoxy D-glucose uptake (FDG-PET). PET Response Criteria in Solid Tumors (PERCIST) was introduced as a potentially more sensitive method of assessing treatment response when compared to assessment based on changes in tumor size alone (4), particularly with therapies that stabilize disease. Imaging with hyperpolarized [1-^{13}C]pyruvate, like FDG-PET, can also be used to detect drug target engagement as well as subsequent tumor cell death (5, 6). We have shown recently that imaging hyperpolarized [1-^{13}C]pyruvate metabolism can be more

sensitive than FDG-PET in detecting reductions in glycolytic flux associated with tumor cell death post treatment (7).

While metabolic imaging may indicate drug target engagement, and in some cases tumor cell death, there is a need for imaging methods that detect tumor cell death more directly post-treatment and that can give an indication of longer term treatment outcomes (8). Fumarate is hydrated in the reaction catalyzed by the intracellular enzyme fumarase to produce malate. Previous ^{13}C magnetic resonance spectroscopic imaging (MRSI) studies with hyperpolarized [1,4-$^{13}C_2$]fumarate in tumor models and in models of myocardial infarction and acute kidney necrosis (9-16) have demonstrated that the production of labeled malate can be used to image cell death in vivo. The increased production of malate was attributed to loss of the plasma membrane permeability barrier in necrotic cells and increased access of hyperpolarized [1,4-$^{13}C_2$]fumarate to fumarase. However, imaging with hyperpolarized ^{13}C-labelled substrates is limited both by the transient nature of the hyperpolarization, which restricts its application to relatively fast metabolic processes, and the requirement for relatively large amounts of ^{13}C-labeled compounds and access to clinical hyperpolarizers, which are expensive. The recent demonstration by De Feyter et al that ^{2}H MRSI can be used to image the metabolism of ^{2}H-labelled substrates in vivo, including in human subjects (17), has provided a potentially lower cost alternative for clinical metabolic imaging. The relatively low sensitivity of ^{2}H detection is compensated by its very short T_1, which means that signal can be acquired rapidly without saturation. The main limitation is the narrow frequency range, which requires the use of relatively high magnetic field strengths. Nevertheless, by collecting a series of rapidly acquired images, the technique is

capable of generating quantitative images of metabolic flux (18). We show here that ^{2}H MRS and MRSI measurements of [2,3-$^{2}H_2$]fumarate conversion to ^{2}H-labeled malate can be used to detect tumor cell death in vivo and that this is potentially a more sensitive method for detecting cell death than ^{13}C MRSI with either hyperpolarized [1-^{13}C]pyruvate or [1,4-$^{13}C_2$]fumarate.

Materials and Methods

More detailed information is give in the Supplementary Information file.

Cell culture

Murine lymphoma EL4 and human colorectal adenocarcinoma Colo205 cells were cultured in RPMI medium (Life Technologies) supplemented with 2 mM L-glutamine and 10% fetal bovine serum (FBS) (Gibco/Thermo Fisher Scientific) and human triple negative breast cancer MDA-MB-231 cells in Dulbecco's Modified Eagle Medium (DMEM) (Gibco) containing 10 % FBS.

Tumor implantation

EL4, MDA-MB-231 or Colo205 cells were injected subcutaneously at 5 x 10^6, 7 x 10^6 and 10 x 10^6 cells respectively. EL4 tumors were allowed to develop for 10 days before imaging, whereas Colo205 and MDA-MB-231 tumors were imaged after 14 days and 35 days respectively. Animals bearing EL4 tumors were treated with etoposide (67 mg/kg of body weight, intraperitoneally), or solvent vehicle (saline) 48 h before imaging. Animals bearing MDA-MB-231 or Colo205 tumors were treated with MEDI3039 (19) (0.8 mg/kg of body weight; intravenously) or solvent vehicle (saline) 24 h before imaging. All animal experiments were carried out in compliance

with project and personal licenses issued by the Home Office, UK and approved by the Cancer Research UK, Cambridge Institute Animal Welfare and Ethical Review Body.

Synthesis of disodium [2,3-$^2H_2$]fumarate and measurement of T_1

Three g of [2,3-$^2H_2$]fumaric acid (Sigma-Aldrich) were dissolved in 8 M NaOH and then freeze-dried. The ^2H T_1s of fumarate, HDO and of DMSO-d6 (3 mM) and formate-d (5 mM), which were used as chemical shift and intensity standards, were measured using an inversion recovery sequence at 147 ms, 199 ms, 719 ms and 1.637 s respectively.

^2H MR spectroscopy measurements on media samples

EL4 cells in suspension were treated with 15 μM etoposide and Colo205 and MDA-MB-231 cells on plates with 10 pM MEDI3039 for 24 h. The cells were then washed in PBS, resuspended at 1 x 10^6 cells/ml in 10 ml culture medium, and 5 mM [2,3-$^2H_2$]fumarate was added. One ml samples were taken at the specified time points and ^2H NMR spectra were acquired The amplitudes of the water, fumarate and malate resonances were normalized to the DMSO-d6 peak, after correction for the slight saturation of the DMSO-d6 resonance, in order to calculate concentrations (17, 18). Absolute concentrations were obtained by correcting for the numbers of deuterons per molecule.

MR spectroscopy and spectroscopic imaging in vivo

Experiments were performed at 7 T (Agilent, Palo Alto, CA) using a 72 mm diameter birdcage volume coil for ^1H transmit and receive (Rapid Biomedical GMBH, Rimpar,

Germany) and a home-built 10 mm diameter single-loop surface coil, located over the tumor, for ^{2}H transmit and receive. The tumors were localized in axial ^{1}H images acquired with a fast spin echo (FSE) pulse sequence. Serial ^{2}H spectra were acquired using a pulse-acquire sequence with a 2 ms BIR4 (20) adiabatic excitation pulse, with nominal flip angle of 67º, a TR of 140 ms and a spoiler gradient on the Z-axis to dephase any residual transverse magnetization. Thirteen, 5 minute spectra were acquired over 65 minutes. Localization of signal to the tumors was achieved by the excitation profile of the surface coil and confirmed by chemical shift images, which showed that signal was largely confined to the tumors. After peak fitting, the intensity of the HDO peak at the first time point was assumed to correspond to the natural abundance of ^{2}H in HDO, which has been estimated to be 10.12 mM in tissue (17, 18). The HDO signal provides an internal reference, which was used to estimate the concentration of deuterated fumarate. The signals were corrected for saturation (15%) by assuming that the T_1s *in vivo* were similar to those measured *in vitro* at 14.1 T and correcting for the number of ^{2}H nuclei in [2,3-$^{2}H_2$]fumarate. The concentration of malate was estimated from the intensity of the upfield resonance and assuming that it has a similar T_1 to the fumarate resonance. The downfield resonance and the HDO peak overlap in vivo, which results in a slight overestimation of the labelled water concentration at later time points. 3D chemical shift images (CSI) were acquired as described in (18). Disodium [2,3-$^{2}H_2$]fumarate was dissolved in water at a concentration of 312.5 mM and infused via a tail vein catheter. The infusion started 5 min after the start of spectral or image acquisition and resulted in 1 g/kg body weight of [2,3-$^{2}H_2$] disodium fumarate infused over a period of 20 min.

MR spectroscopy of blood extracts

EL4 tumor-bearing mice (n = 6) were injected with 1 g/kg [2,3-$^{2}H_2$]fumarate under isoflurane anesthesia. Blood was taken via cardiac puncture at 20 (n=3) and 70 (n=3) min after fumarate injection. Blood from two more mice was taken without prior injection of fumarate. The blood was vortexed in ice-cold 2M perchloric acid (PCA) for 30 s, centrifuged at 13,000 g at 4 °C for 15 min and then neutralized with ice-cold 2M KOH. The neutralized extract was then centrifuged for 10 min at 13,000 g and 200 µl of the supernatant added to 300 µl H_2O and a formate-d standard added to a final concentration of 4 mM. ^{2}H NMR spectra were acquired using the same acquisition parameters as used for the media samples, but with a TR of 3 s. Concentrations were calculated by comparison of the signal intensities with that of the formate-d standard, after correction for slight signal saturation in the latter. A standard for proton NMR measurements (3-(trimethylsilyl)-2,2,3,3-tetradeuteropropionic acid) was then added to give a final concentration of 1 mM, together with 50 µl $^{2}H_2O$, and ^{1}H spectra were acquired with water pre-saturation and a flip angle of 90º into 16384 data points, with a spectral width of 7788 Hz and a repetition time of 8 s.

MR spectroscopy of tissue extracts

EL4 tumor-bearing mice were injected with 1 g/kg [2,3-$^{2}H_2$]fumarate (n=3) or PBS (n=3) under isoflurane anesthesia and after 20 min the animals were killed by cervical dislocation and tumor, kidney, liver, and muscle tissue were freeze-clamped in liquid nitrogen-cooled tongs. For measurements on heart muscle, non-tumor bearing C57BL/6J mice (n=8) were either injected with 1 g/kg [2,3-$^{2}H_2$]fumarate or PBS (n=3) under isoflurane anesthesia and after 20 (n=3) and 60 min (n = 2) the animals were killed by cervical dislocation. The chest cavity was opened to expose

the heart, the descending aorta, inferior vena cava, and pulmonary trunk were cut, and the heart immediately flushed anterograde with ice-cold PBS by inserting a cannula into the apex of the right ventricle to inhibit contraction and to flush blood from the chambers. Remaining blood was aspirated from the ventricles and the heart submerged in a dish filled with ice-cold oxygenated Krebs-Henseleit buffer before the tissue was freeze-clamped in liquid nitrogen-cooled tongs. The frozen samples were homogenized in ice-cold 2M PCA using a Precellys Cryolys Evolution tissue homogenizer (Bertin Instruments) and neutralized with 2M KOH. After centrifugation for 15 min at 13,000 *g*, 200 µl of the supernatant was mixed with 300 µl of H_2O and a formate-d standard added to a final concentration of 4 mM. ^2H NMR spectra were acquired using the same acquisition parameters as used for the blood samples. Following the ^2H NMR measurements, a standard for proton NMR measurements, 3-(trimethylsilyl)-2,2,3,3-tetradeuteropropionic acid was added at a final concentration of 1 mM, together with 50 µl of ^2H_2O, and ^1H spectra were acquired, as for the blood samples.

^2H MR spectroscopy of erythrocyte suspensions

Erythrocytes were diluted to a haematocrit of ~40% in Krebs-Henseleit buffer (NaCl 118.5; $NaHCO_3$ 25.0; KCl 4.7; KH_2PO_4 1.2; $MgSO_4$ 1.2; glucose 11; $CaCl_2$ 2.4; mmol/L, pH 7.4) gassed with 95% O_2 / 5% CO_2. ^2H NMR spectra were acquired at 310 K following the addition of 8 mM [2,3-$^2H_2$]fumarate and 5 mM formate-d6. Spectra were acquired using a 90° pulse, a repetition time of 2 s and were the sum of 150 transients.

Dynamic contrast-enhanced MRI

EL4, MDA-MB-231 and Colo205 tumor-bearing animals (n = 3 per group) underwent dynamic contrast-enhanced (DCE)-MRI before and either 48 (EL4) or 24 (MDA-MB-231 and Colo205) hours after treatment with etoposide (EL4) or MEDI3039 (MDA-MB-231 and Colo205). Images were acquired at 9.4 T using a 40 mm diameter ^{1}H volume coil. Baseline T_1 measurements were made using an inversion recovery-fast spin echo sequence. A series of 500 spoiled gradient echo images (2 averages, 5 seconds per set of 3 images) were acquired. Dotarem, at 200 μmoles/kg (Gadoteric acid, Guerbet), was injected via a tail vein after the 10th image. Signals from the image series were converted, on a pixel-by-pixel basis, to a contrast-agent concentration by assuming an R_1 relaxivity of the contrast agent of 2.7 $s^{-1}mM^{-1}$ (21).

Western blotting

Freeze-clamped tumor samples were homogenized in 10 μL/mg RIPA buffer (ThermoFisher Scientific) containing cOmplete mini EDTA-free protease inhibitor (Sigma Aldrich). Membranes were probed with a rabbit polyclonal IgG fumarase antibody (ThermoFisher) and a mouse monoclonal GAPDH antibody (Abcam) and detected using IRDye 800CW Goat anti-Rabbit IgG (LI-COR) and IRDye 680LT Goat anti-Mouse IgG antibodies (LI-COR).

Measurements of fumarase activity and ATP concentration in tissue extracts

Fumarase activity and ATP concentrations were determined using colorimetric (ab196992, Abcam) and fluorometric kits (ab83355, Abcam), respectively. At 48 h after treatment with etoposide (EL4), and 24 h after treatment with MEDI3039 (MDA-MB-231 and Colo205) or drug vehicle, tumors were freeze-clamped and either homogenized in ice-cold 4 M PCA (ATP assay) or in assay buffer (fumarase assay)

using a Precellys 24 homogenizer (Stretton Scientific). The ATP extracts were neutralized with 8 M KOH. Fumarase activity was assayed spectrophotometrically by measuring the conversion of malate to fumarate from the increase in absorbance at 450 nm, according to the manufacturer's instructions. ATP concentration was determined fluorometrically (Ex/Em = 535/587 nm), again according to the manufacturer's instructions. Both measurements were made using a PHERAstar FS microplate reader (BMG Labtech).

Histology and immunohistochemistry

Sections of formalin-fixed paraffin-embedded tumors (10 μm) were stained with hematoxylin and eosin and with a rabbit monoclonal anti-CC3 antibody (Cell Signaling Technology) and a donkey anti-rabbit secondary biotinylated antibody (Jackson ImmunoResearch Laboratories). Sections were also stained using TdT-mediated dUTP Nick- End Labeling (TUNEL) (PromegaBenelux BV). Slides were scanned at 20x magnification with a resolution of 0.5 μm per pixel on an Aperio AT2 (Leica Biosystems).

Statistical analysis

Statistical and graphical analyses was performed using Prism v8 (GraphPad). Data are shown as mean ± SD, unless stated otherwise. Analysis of variance was used for multiple comparisons of groups to determine significance. A paired or unpaired Student *t* test was used for single-parameter comparisons. P values are summarized in figure tables as: * $P = 0.01 – 0.05$; ** $P = 0.001 – 0.01$; *** $P = 0.0001 – 0.001$; **** $P < 0.0001$.

Results

Deuterated fumarate metabolism detects tumor cell death in vitro

Cultured murine lymphoma cells (EL4) (Figure 1) were treated with 15 μM etoposide or drug vehicle (control) for 24 h. Cell viability was 90 ± 3% prior to treatment and 9 ± 4% at 24 hours post-etoposide treatment. Five mM [2,3-$^2H_2$]fumarate was added to the cell suspensions and samples taken for ^2H NMR measurements of the deuterated fumarate, malate and water concentrations. As early as one minute after [2,3-$^2H_2$]fumarate addition, etoposide-treated cells showed increased malate production (Figure 1A,B). The deuterium-labeled malate concentration was 1.3 ± 0.4 mM in drug-treated cell suspensions as compared to 0.17 ± 0.04 mM in controls (P < 0.0001, n=3 per group). The labeled malate production rate was significantly higher (P = 0.0004) in the etoposide-treated group (34.1 ± 1.8 fmol/min/cell) compared to controls (12.9 ± 2.7 fmol/min/cell) (Fig. 1**G**). Similar results were obtained in colorectal (Colo205) (Fig. 1H-J) and triple negative breast cancer (MDA-MB-231) cells (Fig. 1K-M). The rates of malate production post-treatment were higher in Colo205 cells (6.1 ± 0.2 fmol/min/cell) (Fig. 1J) and MDA-MB-231 cells (9.1 ± 0.7 fmol/min/cell) (Fig. 1M) compared to untreated controls (Colo205, 2.1 ± 0.6 fmol/min/cell; MDA-MB-231, 2.2 ± 0.4 fmol/min/cell). These rates were much lower than those observed in treated EL4 cells, however there was much less cell death, with the viabilities of these two cell lines post treatment being much higher (Colo205, 56 ± 2.4%, MDA-MB-231, 55 ± 4.1%) than in EL4 cells (9 ± 4%). The rates of water labeling, which can be explained by TCA cycle activity (17, 18, 22, 23), were not significantly affected by treatment. The rate in untreated EL4 cells was 30.1 ± 2.4 fmol/min/cell, in MDA-MB-231 cells 20.3 ± 4.9 fmol/min/cell and in Colo205 cells 16.7 ± 5.8 fmol/min/cell, whereas in treated cells the corresponding rates were 35.6

± 1.2, 18.7 ± 4.9 and 19.3 ± 2.4 fmol/min/cell respectively, indicating that there was retention in the necrotic cells of the activities of those enzymes responsible for exchange of fumarate deuterons with water. Moreover, these rates were similar to the rates of fumarate utilization, which in untreated EL4 cells was 31.9 ± 3.8 fmol/min/cell, in MDA-MB-231 cells 10.1 ± 5.1 fmol/min/cell and in Colo205 cells 17.6 ± 3.1 fmol/min/cell and in the treated cells 38.9 ± 2.4, 12.3 ± 3.9 and 20.7 ± 6.9 fmol/min/cell respectively.

Deuterated fumarate metabolism detects tumor cell death in vivo

Deuterium-labeled fumarate, malate and water concentrations were monitored in EL4, MDA-MB-231 and Colo205 tumors using localized ^{2}H spectroscopy measurements following intravenous injection of 1 g/kg [2,3-$^{2}H_2$]-disodium fumarate (Figure 2). In all three implanted tumor models there was a significant increase in labeled malate concentration following drug treatment, which in the EL4 tumors was confirmed by measurements of the concentrations in freeze-clamped tumor extracts (Table 1). In untreated tumors the concentration of [2,3-$^{2}H_2$]malate, determined by ^{2}H NMR, was only 10% of the unlabeled concentration, determined by ^{1}H NMR, whereas in treated tumors the total malate concentration increased ~7x, of which ~30% was deuterium labeled (Table 1). In both the untreated and treated tumors the fumarate was ~50% labeled, indicating that there had been substantial solvent exchange of fumarate deuterons. The tumor malate/fumarate and malate/HDO signal ratios measured in vivo at 48 h (EL4) or 24 h (MDA-MB-231 and Colo205) after treatment are shown in Figure 3.

The labeled malate concentration in etoposide-treated EL4 tumors (Figure 2 and Table 1) was ~4x the labeled malate concentration in blood (Table 2). Moreover, the

labeled malate concentration in blood increased markedly posttreatment, consistent with the treated tumor being the major source of labeled blood malate. Labeled malate was undetectable in liver and muscle but present in kidney at much higher concentration than in blood, both before and after treatment. The increase in malate concentration in the kidney post treatment was comparable with the increase in the blood concentration. The labeled fumarate concentration in the kidney pretreatment was similar to the blood concentration and approximately 2x that in the tumor and 5x that in the liver. There were only very low concentrations of labeled fumarate in skeletal muscle. Heart muscle takes up fumarate rapidly (24) and we observed labelled malate concentrations in this tissue that exceeded the blood concentration in untreated animals (Tables 1 & 2). The labelled water concentration in heart muscle was similar to that in the blood pool. Erythrocytes will also take up fumarate and produce malate on the time scale of the experiments shown here (25). Incubation of erythrocytes with [2,3-$^{2}H_2$]fumarate produced concentrations of labelled malate comparable to those observed in the heart. However, there was no increase in water labelling (Table 3), reflecting the low levels of TCA cycle enzymes in these cells (26).

The tumor fumarate signal in the EL4 and MDA-MB-231 tumor models increased significantly following drug treatment (Figure 2A-D), implying that there was increased perfusion since the blood fumarate concentration did not change significantly following etoposide treatment (Table 2). To confirm changes in tumor perfusion, dynamic contrast enhanced MRI measurements were performed in EL4, MDA-MB-231 and Colo205 tumor-bearing mice.

DCE-MRI showed an increase in perfusion of EL4 and MDA-MB-231 tumors after treatment

In separate cohorts of MDA-MB-231 (n=3) EL4 (n=3) and Colo205 (n=3) tumor-bearing mice, DCE-MRI was used to assess tumor perfusion following drug treatment (Figure S1). Tumor gadolinium (Gd^{3+}) concentrations pre- (0.25 $\pm$ 0.02 mM) and post-treatment (0.27 $\pm$ 0.016 mM) showed no difference (*P* = 0.9953) in the Colo205 tumor model (Fig.4B), but were increased slightly by treatment in MDA-MB-231 and EL4 tumor-bearing mice (Fig. 4D,F), increasing from 0.19 $\pm$ 0.05 to 0.39 $\pm$ 0.09 mM (P = 0.0021) and 0.18 $\pm$ 0.01 to 0.59 $\pm$ 0.08 (P = 0.0001), respectively at approximately 10 minutes after intravenous injection of the contrast agent.

Fumarase activity is decreased in cells and tumors by drug treatment

Increased conversion of fumarate to malate has been attributed to compromised plasma membrane integrity in necrotic cells and consequently increased access of fumarate to the enzyme (9). To confirm this, we measured fumarase activity in drug-treated cells in culture and in drug-treated tumors in vivo (Figure 4). Enzyme activity was decreased in cells, and enzyme activity and protein levels were decreased in tumors, by drug treatment, confirming loss of plasma membrane integrity and leakage of the enzyme from the cell (9, 15).

Confirmation of cell death in drug-treated tumors

Cell death in drug-treated tumors was confirmed by measuring tumor size and ATP concentrations (Figure 5) and by histological assessment of the levels of cleaved capase 3 (CC3) and DNA damage (TUNEL) (Figure 6). Although there was no significant decrease in the size of MDA-MB-231 and Colo205 tumors after

MEDI3039 treatment, there were nevertheless significant decreases in tumor ATP content and increases in CC3 and TUNEL staining, as we have observed previously in these tumor models following MEDI3039 treatment (7). EL4 tumors showed a significant decrease in volume, from 0.7 ± 0.3 cm^3 to 0.5 ± 0.1 cm^3 at 48 h after etoposide treatment, and increases in CC3 and TUNEL staining.

^2H imaging of cell death using [2,3-$^2H_2$]fumarate

A fast, dynamic 3D chemical shift imaging sequence was used to capture spatial information about the conversion of [2,3-$^2H_2$]fumarate to [2,3-$^2H_2$]malate in implanted EL4 tumors in vivo following a bolus injection of labelled fumarate (1g/kg) into tumor-bearing mice, both pre- and post-treatment (Figure 7). No malate signal was detected pre-treatment whereas significant malate production was observed 48 h after etoposide treatment. The signal was localized to the tumor area. The fumarate concentration also increased in the tumor post-treatment in agreement with the DCE MRI, tissue extract and spectroscopy data.

Discussion

^{13}C MR spectroscopy and spectroscopic imaging of [1,4-$^{13}C_2$]malate production from hyperpolarized [1,4-$^{13}C_2$]fumarate has been used previously to detect early evidence of tumor cell death in EL4 tumors following treatment with etoposide (9) and in MDA-MB-231 tumors following treatment with doxorubicin (10). Production of labelled malate by necrotic cells has been attributed to a compromised plasma membrane permeability barrier allowing fumarate to rapidly gain access to cell fumarase with

consequent conversion to malate within the short lifetime of the ^{13}C spin polarization, thus providing a positive marker of tumor cell necrosis. We have shown here, using deuterium labelled fumarate, that the limited lifetime of the ^{13}C spin polarization, which is of the order of 1 – 2 minutes in vivo (27, 28), is not a prerequisite for an effective cell death measurement using labeled fumarate. Untreated tumors had only low levels of [2,3-$^{2}H_2$]malate at 60 minutes after injection of [2,3-$^{2}H_2$]fumarate, whereas in treated tumors elevated levels of [2,3-$^{2}H_2$]malate were detected within 15 minutes. Increased malate production in dead or dying cells cannot be explained by increased fumarase activity. As was observed previously in studies with hyperpolarized [1,4-$^{13}C_2$]fumarate (9), enzyme activity decreased in drug-treated cells and tumors reflecting leakage of the enzyme from necrotic cells into the cell culture medium and tumor interstitial space. Increased malate production can also not be explained by increased delivery of labelled fumarate to the tumor post treatment. Although the EL4 and MDA-MB-231 tumors both showed significantly higher levels of [2,3-^{2}H]fumarate post treatment, which DCE-MRI measurements showed was due to increased perfusion, this is unlikely to be responsible for the increased [2,3-$^{2}H_2$]malate signal post treatment since the fumarate concentration in these tumors, both pre- and post-treatment, was in considerable excess of the Km of fumarase for fumarate, which has been measured at 5 μM (29). Moreover, Colo205 tumors showed a similar increase in the levels of labelled malate post-treatment with no change in tumor perfusion, as assessed from the concentrations of [2,3-$^{2}H_2$]fumarate and gadolinium contrast agent. Furthermore, detecting cell death through an increase in the malate/fumarate signal ratio corrects for the effects of any changes in perfusion since the fumarate signal provides a measure of this.

While fumarate was taken up by viable cells, as evidenced by water labeling observed in the cell experiments, there was no subsequent accumulation of labeled malate, which we only observed in drug-treated cells and tumors. Deuterons can be lost from [2,3-$^{2}H_{2}$]fumarate in the sequential reactions catalyzed by fumarase and malate dehydrogenase and subsequent keto-*enol* tautomerization of the oxaloacetate produced (30). The similarity between the rate of fumarate consumption and water labelling in all three cell lines suggests that fumarate is taken up by viable cells and metabolized to malate and subsequently to oxaloacetate. The absence of a significant increase in the rate of water labelling in Colo205 and MDA-MB-231 cells following drug treatment, when >40% of the cells had become necrotic, suggests that in these cells the rate is limited by malate dehydrogenase activity and the rate of oxaloacetate tautomerization. The rates of fumarate utilization increased in all three cell lines following treatment, consistent with the proposal that the increase in malate labeling is due to increased access of fumarate to fumarase in necrotic cells. However, there was no concordance between the increase in the rates of fumarate utilization and malate labeling post-treatment across the three cell lines (7 versus 21 fmols/min/cell respectively in EL4 cells, 3 versus 4 fmols/min/cell in Colo205 cells and 2 versus 7 fmols/min/cell in MDA-MB-231 cells), suggesting that the observation of increased malate labeling may also be due to an increase in the steady state level of malate in drug-treated cells resulting from reduced consumption in the TCA cycle. ^{2}H and ^{1}H NMR measurements on EL4 tumor extracts showed a large increase in the concentrations of labeled and unlabeled malate post-treatment. In untreated tumors only ~10% of the malate was deuterium labeled, which is likely due to production of malate from other carbon sources and also exchange of deuterium label in malate with solvent water in the reversible

reaction catalyzed by malate dehydrogenase and subsequent keto-*enol* tautomerization of oxaloacetate. Following etoposide treatment, the total malate concentration increased 7x, of which 30% was deuterium labeled. Only ~50% of the fumarate in the tumors was deuterium labeled, showing that there had been substantial solvent exchange in the tumor and other body tissues.

Measurements in tissue extracts showed high levels of labelled fumarate in the kidneys (11 μmols/g), presumably reflecting rapid renal excretion, as we have observed previously with hyperpolarized [1,4-$^{13}C_2$]fumarate (15), with lower levels in the tumor and lower levels still in the liver and heart (Table 1). Labeled fumarate in the liver and heart muscle can be explained, at least in part, by labeled fumarate present in the blood pool. With a blood [2,3-$^{2}H_2$]fumarate concentration of 12 mM at 20 min after injection (Table 2), and using blood volumes in mouse liver and kidney of ~0.2 mL/g tissue (31), and accessible volumes (vascular plus interstitial) in liver and heart muscle of ~0.2 mL/g (32) gives a calculated concentration of labelled fumarate in the liver, kidney and heart muscle blood pools of ~2.4 μmols/g tissue. This is similar to the measured tissue concentration of 2.1 μmols/g in liver, although above that measured in heart, which was 1.2 μmols/g. The evidence that fumarate is largely present in the liver blood pool and not in the liver cells is further supported by the absence of detectable [2,3-$^{2}H_2$]malate in liver. The highest malate concentration in the blood would contribute only ~0.1 μmols/g liver and was at the limit of detection in these ^{2}H NMR measurements on liver extracts (Table 1). However, the labelled malate concentration in heart muscle was 0.3 μmols/g, 10x that in the blood and indicating substantial uptake and metabolism of fumarate in heart muscle, as has been observed previously (24). This may explain why the

fumarate concentration in the heart was lower than that expected based on the concentration in the blood pool. Fumarate uptake and metabolism in the heart may also have contributed to the observed water labeling in this tissue. However, since the labeled water concentration was similar to that in the blood we cannot distinguish between labeled water generated in the heart and that washed in from other tissues. The labelled malate concentration in the kidney at 20 min after labelled fumarate injection (0.6 μmols/g) was much higher than can be accounted for by the [2,3-$^{2}H_2$]malate concentration in the blood (0.03 mM). Some of this labelled malate may have been produced in the kidney but some may have been produced elsewhere in the body and was undergoing excretion via the kidneys. In etoposide-treated EL4 tumor-bearing mice the kidney malate concentration more than doubled to 1.3 μmols/g. Although the blood concentration also increased, to 0.5 mM, again the blood pool can make only a very small contribution to the total kidney malate concentration. Some of this malate is presumably malate that has washed out of the treated tumor, where the labelled malate concentration increased from 0.08 μmols/g prior to treatment to 1.8 μmols/g post-treatment, at 20 minutes after injection of [2,3-$^{2}H_2$]fumarate. Importantly the malate concentration in the tumor at this time point was ~4x higher than the blood concentration, demonstrating that the malate had been produced by cell death in the tumor rather than being washed in from elsewhere in the body.

The production of malate from fumarate makes fumarate a positive contrast agent for detecting cell death and in principle should be more sensitive for detecting cell death than imaging techniques that rely on a decrease in signal, for example a decrease in tumor lactate labelling in animals injected with hyperpolarized [1-^{13}C]pyruvate (5, 7).

In the same Colo205 and MDA-MB-231 tumor models that were used here we have shown previously that treatment with MEDI3039 resulted in a decrease in lactate labelling from hyperpolarized [1-^{13}C]pyruvate (expressed as the ^{13}C lactate/pyruvate signal ratio) of 42.2 ± 15.9% and 36.3 ± 18.6% in Colo205 and MDA-MB-231 tumors respectively (7). There was an increase in TUNEL staining in the Colo205 tumors, from 8.0 ± 6.7% to 19.4 ± 6.3% and in the MDA-MB-231 tumors, from 6.6 ± 2.0% to 21.1 ± 6.1%. Expressing the percentage decrease in lactate labelling as a ratio of the increase in the percentage of cell death gives values of 3.7 and 2.5 for Colo205 and MDA-MB-231 tumors respectively. In the study presented here, MEDI3039 treatment resulted in an increase in the [2,3-$^{2}H_2$]malate/[2,3-$^{2}H_2$]fumarate signal ratio from 0.016 ± 0.04 to 0.28 ± 0.26 in Colo205 tumors, a 1650 % increase, and an increase from 0.019 ± 0.03 to 0.25 ± 0.23 in MDA-MB-231 tumors, an increase of 1216%. TUNEL staining increased from 6.3 ± 2.3% to 77.6 ± 5.6% in Colo205 tumors and from 5.0 ± 1.7% to 56.4 ± 3.9% in MDA-MB-231 tumors. Expressing the percentage increase in malate labelling as a ratio of the increase in the percentage of cell death gives values of 23 and 24 for Colo205 and MDA-MB-231 tumors respectively. Therefore, monitoring malate production from labelled fumarate is indeed a more sensitive method for detecting cell death than monitoring the decrease in lactate labelling from hyperpolarized [1-^{13}C]pyruvate. This assessment of sensitivity, however, does not take into account the much lower signal-to-noise ratio (SNR) in the ^{2}H spectra, which also has a large effect on our estimate of the sensitivity of the deuterated fumarate experiment for detecting cell death given the very low intensity of the malate ^{2}H signal in the untreated tumors. The SNRs of the most intense malate peak in the ^{2}H spectra of treated Colo205 and MDA-MB-231 tumors were 1.7±0.6 and 2.3±0.9 respectively whereas the lactate SNRs in the ^{13}C

spectra of these tumors published previously were 44±7 (7) and 46±8 respectively (10). The differences in SNR between the ^{2}H and ^{13}C experiments will also depend on coil configuration and performance.

We have shown previously that detecting cell death with hyperpolarized [1,4-^{13}C]fumarate is more effective than diffusion-weighted ^{1}H MRI at detecting low levels of diffuse necrosis (11). Treatment of EL4 tumors with an anti-vascular drug that resulted in small areas of necrosis at 6 hours after treatment resulted in a significant increase in labeled malate production with no change in the apparent diffusion coefficient (ADC) of tissue water in a diffusion-weighted imaging experiment. This was consistent with a previous study, which showed in tumors with small and diffuse regions of necrosis that there can be no change in ADC, even with necrotic fractions of up to 40% (33). Malate detection effectively integrates cell death over the whole imaging voxel, since it is a positive contrast agent, whereas with small and diffuse regions of necrosis in the image voxel, detection of cell death using diffusion-weighted MRI involves measuring relatively small increases in the water ADC. Assessing cell death in vivo using [2,3-$^{2}H_2$]fumarate is simpler than with hyperpolarized [1,4-^{13}C]fumarate since the method does not require a hyperpolarizer, and as a result is also less expensive to implement. However, it does require much higher concentrations of labelled fumarate; 0.4 mL of 312 mM [2,3-$^{2}H_2$]fumarate was used here as compared to 0.2 mL of 20 mM hyperpolarized [1,4-^{13}C]fumarate used previously (9). Despite the higher fumarate concentration, the SNR of the most intense [2,3-^{2}H]malate signal was only 2.9±0.2 in the spectra of etoposide-treated EL4 tumors, which were the sum of 2,142 transients acquired over 5 minutes using a 67º pulse and a repetition time of 0.14 s and 4.5±0.5 in the sum of

the 13 spectra acquired over 65 minutes. Signal was acquired from the sensitive volume of the surface coil, which imaging experiments showed included mainly tumor tissue. Contrast this with ^{13}C spectroscopy measurements of hyperpolarized [1,4-^{13}C]fumarate metabolism in etoposide-treated EL4 tumors where the malate SNR in spectra, which were the sum of 60 transients acquired over 3 minutes using a 10° pulse, a repetition time 3 s, and a slice thickness of 5 mm, was 17 (9). Increasing the concentration of [2,3-$^{2}H_2$]fumarate further was not possible as this started to affect breathing and heart rates, which may have been a consequence of the sodium ion present in the preparation. The LD_{50} for i.v. sodium chloride in mice is 645 mg/kg, which is approximately 2.8 osmol/L; we injected 1 osmol/L disodium fumarate. However, ^{2}H MRS measurements of [2,3-^{2}H]malate production from [2,3-^{2}H]fumarate appear to be an intrinsically more sensitive method for detecting cell death than ^{13}C MRS measurements of [1,4-^{13}C]malate production from hyperpolarized [1,4-^{13}C]fumarate. In EL4 tumor-bearing mice injected with hyperpolarized [1,4-^{13}C]fumarate the rate constant describing labelled malate production in the tumor increased by a factor of 2.4 following etoposide treatment and the ratio of the areas under the malate and fumarate labelling curves increased by a factor of 1.6, where this was the result of an increase in tumor cell necrosis from ~5% to ~30% (9). Whereas in this study, in EL4 tumor-bearing mice injected with [2,3-$^{2}H_2$]fumarate, the ratio of the areas under the malate and fumarate labelling curves increased by a factor of 10, increasing from 0.02 ± 0.02 to 0.16 ± 0.14 (P=0.0024, n=3) following etoposide treatment, with the estimated levels of tumor cell necrosis increasing from 15 ± 5% to 59 ± 6%. This greater sensitivity of the ^{2}H experiment for detecting cell death can be explained by the extended period over which the accumulation of labeled malate is measured, 65 mins, as compared to just

3 min in the case of the hyperpolarized ^{13}C experiment, which is limited by the short lifetime of the ^{13}C hyperpolarization.

The chemical shift separation of the fumarate, water and malate resonances and the concentrations of fumarate and malate observed in the tumors suggest that this technique for detecting tumor cell death post-treatment could translate to the clinic. De Feyter et al (17) observed partially resolved resonances from water and glucose at 4.8 and 3.8 ppm respectively, and resolved resonances from Glx and lactate at 2.4 and 1.4 ppm respectively in the human brain at 4 T. Here, at 7 T, we observed partially resolved resonances from fumarate and water at 6.5 and 4.8 ppm respectively and a resolved resonance from malate at 2.4 ppm. Since the fumarate and malate resonances show larger chemical shift differences from their immediately adjacent resonances than the water, glucose, Glx and lactate resonances, and since the resolution of the ^{2}H spectra scales linearly with magnetic field (34), then we would expect the fumarate and malate resonances to be resolved from each other and from the water resonance at 3 T, a field more widely used in the clinic. De Feyter et al detected glucose and Glx at concentrations of up to 1.5 and 2 mM respectively in 20 × 20 × 20 mm^3 voxels in the normal human brain at 4 T. Here we detected fumarate and malate concentrations of around 5 mM. The expected decrease in sensitivity in going from 4 to 3 T is ~40% (34) and therefore we expect to be able to detect fumarate and malate at 3 T, even if the fumarate dose has to be decreased for human studies.

In conclusion, this study has demonstrated that ^{2}H spectroscopy and spectroscopic imaging of [2,3-$^{2}H_2$]fumarate metabolism can be used to detect tumor cell death

post-treatment, before there are detectable changes in tumor size. Translation of this technique to the clinic could offer a new approach to detecting early tumor responses to therapy and potentially to detect cell death in other conditions, such as acute kidney tubular necrosis, and myocardial infarction.

Acknowledgments

The authors acknowledge the support of the Cancer Research UK Cambridge Institute core facilities, in particular the biological resources unit, histopathology, and preclinical imaging sections. We would also like to thank Mike Mitchell, Toby Fewster, Jodi Miller, Sarah McGuire, and Madhu Basetti for their help. The work was supported by grants from Cancer Research UK (C197/ A17242, C197/A16465, C9685/A25177). FH is in receipt of a Cambridge European Scholarship from the Cambridge Trust.

References

1. Eisenhauer EA*, et al.* (2009) New response evaluation criteria in solid tumours: revised RECIST guideline (version 1.1). *Eur J Cancer* 45(2):228-247.
2. Brindle K (2008) New approaches for imaging tumour responses to treatment. *Nat Rev Cancer* 8(2):94-107.
3. Gerwing M*, et al.* (2019) The beginning of the end for conventional RECIST - novel therapies require novel imaging approaches. *Nat Rev Clin Oncol* 16(7):442-458.
4. Wahl RL, Jacene H, Kasamon Y, & Lodge MA (2009) From RECIST to PERCIST: Evolving Considerations for PET response criteria in solid tumors. *J Nucl Med* 50 Suppl 1(Suppl 1):122s-150s.
5. Day SE*, et al.* (2007) Detecting tumor response to treatment using hyperpolarized ^{13}C magnetic resonance imaging and spectroscopy. *Nat Med* 13(11):1382-1387.
6. Witney TH*, et al.* (2009) A comparison between radiolabeled fluorodeoxyglucose uptake and hyperpolarized ^{13}C-labeled pyruvate utilization as methods for detecting tumor response to treatment. *Neoplasia* 11(6):574-582, 571 p following 582.

7. Hesketh RL*, et al.* (2019) Magnetic Resonance Imaging Is More Sensitive Than PET for Detecting Treatment-Induced Cell Death-Dependent Changes in Glycolysis. *Cancer Res* 79(14):3557-3569.
8. Neves AA & Brindle KM (2014) Imaging cell death. *J Nucl Med* 55(1):1-4.
9. Gallagher FA*, et al.* (2009) Production of hyperpolarized [1,4-$^{13}C_2$]malate from [1,4-$^{13}C_2$]fumarate is a marker of cell necrosis and treatment response in tumors. *Proc Natl Acad Sci U S A* 106(47):19801-19806.
10. Witney TH*, et al.* (2010) Detecting treatment response in a model of human breast adenocarcinoma using hyperpolarised [1-^{13}C]pyruvate and [1,4-$^{13}C_2$]fumarate. *Br J Cancer* 103(9):1400-1406.
11. Bohndiek SE*, et al.* (2010) Detection of Tumor Response to a Vascular Disrupting Agent by Hyperpolarized C-13 Magnetic Resonance Spectroscopy. *Mol. Cancer Ther.* 9(12):3278-3288.
12. Bohndiek SE, Kettunen MI, Hu DE, & Brindle KM (2012) Hyperpolarized C-13 Spectroscopy Detects Early Changes in Tumor Vasculature and Metabolism after VEGF Neutralization. *Cancer Research* 72(4):854-864.
13. Mignion L*, et al.* (2014) Monitoring chemotherapeutic response by hyperpolarized ^{13}C-fumarate MRS and diffusion MRI. *Cancer Res* 74(3):686-694.
14. Düwel S*, et al.* (2016) Multiparametric human hepatocellular carcinoma characterization and therapy response evaluation by hyperpolarized ^{13}C MRSI. *NMR in biomedicine* 29(7):952-960.
15. Clatworthy MR*, et al.* (2012) Magnetic resonance imaging with hyperpolarized [1,4-$^{13}C_2$]fumarate allows detection of early renal acute tubular necrosis. *Proc Natl Acad Sci U S A* 109(33):13374-13379.
16. Miller JJ*, et al.* (2018) Hyperpolarized [1,4-$^{13}C_2$]Fumarate Enables Magnetic Resonance-Based Imaging of Myocardial Necrosis. *JACC Cardiovasc Imaging* 11(11):1594-1606.
17. De Feyter HM*, et al.* (2018) Deuterium metabolic imaging (DMI) for MRI-based 3D mapping of metabolism in vivo. *Sci Adv* 4(8):eaat7314.
18. Kreis F*, et al.* (2020) Measuring Tumor Glycolytic Flux in Vivo by Using Fast Deuterium MRI. *Radiology* 294(2):289-296.
19. Greer YE*, et al.* (2019) MEDI3039, a novel highly potent tumor necrosis factor (TNF)-related apoptosis-inducing ligand (TRAIL) receptor 2 agonist, causes regression of orthotopic tumors and inhibits outgrowth of metastatic triple-negative breast cancer. *Breast Cancer Res* 21(1):27.
20. Garwood M & DelaBarre L (2001) The return of the frequency sweep: designing adiabatic pulses for contemporary NMR. *J Magn Reson* 153(2):155-177.
21. Lee H*, et al.* (2018) Quantitative Gd-DOTA uptake from cerebrospinal fluid into rat brain using 3D VFA-SPGR at 9.4T. *Magnetic resonance in medicine* 79(3):1568-1578.
22. Lu M, Zhu XH, Zhang Y, Mateescu G, & Chen W (2017) Quantitative assessment of brain glucose metabolic rates using in vivo deuterium magnetic resonance spectroscopy. *J Cereb Blood Flow Metab* 37(11):3518-3530.
23. Aguayo JB, McLennan IJ, Graham C, Jr., & Cheng HM (1988) Dynamic monitoring of corneal carbohydrate metabolism using high-resolution deuterium NMR spectroscopy. *Exp Eye Res* 47(2):337-343.

24. Laplante A, Vincent G, Poirier M, & Des Rosiers C (1997) Effects and metabolism of fumarate in the perfused rat heart. A ^{13}C mass isotopomer study. *The American journal of physiology* 272(1 Pt 1):E74-82.
25. Simpson RJ, Brindle KM, & Campbell ID (1982) Spin echo proton NMR studies of the metabolism of malate and fumarate in human erythrocytes: Dependence on free NAD levels. *Biochimica et Biophysica Acta (BBA) - Molecular Cell Research* 721(2):191-200.
26. Dajani RM & Orten JM (1958) [A study of the citric acid cycle in erythrocytes]. *The Journal of biological chemistry* 231(2):913-924.
27. Brindle KM (2015) Imaging metabolism with hyperpolarized ^{13}C-labeled cell substrates. *J Am Chem Soc* 137(20):6418-6427.
28. Hesketh RL & Brindle KM (2018) Magnetic resonance imaging of cancer metabolism with hyperpolarized ^{13}C-labeled cell metabolites. *Curr Opin Chem Biol* 45:187-194.
29. Teipel JW, Hass GM, & Hill RL (1968) The substrate specificity of fumarase. *The Journal of biological chemistry* 243(21):5684-5694.
30. Englard S (1959) Studies on the mechanism of the citrate condensing enzyme reaction. *The Journal of biological chemistry* 234(5):1004-1006.
31. Kaliss N & Pressman D (1950) Plasma and blood volumes of mouse organs, as determined with radioactive iodoproteins. *Proc Soc Exp Biol Med* 75(1):16-20.
32. Mandikian D*, et al.* (2018) Tissue Physiology of Cynomolgus Monkeys: Cross-Species Comparison and Implications for Translational Pharmacology. *The AAPS Journal* 20(6):107.
33. Lyng H, Haraldseth O, & Rofstad EK (2000) Measurement of cell density and necrotic fraction in human melanoma xenografts by diffusion weighted magnetic resonance imaging. *Magnetic resonance in medicine* 43(6):828-836.
34. de Graaf RA*, et al.* (2020) On the magnetic field dependence of deuterium metabolic imaging. *NMR in biomedicine* 33(3):e4235.

Tables

		Control		Etoposide-treated	
		Concentrations of deuterated species			
	HDO (µmols/g)	**[2,3-$^2H_2$]fumarate** (µmols/g)	**[2,3-$^2H_2$]malate** (µmols/g)	**[2,3-$^2H_2$]fumarate** (µmols/g)	**[2,3-$^2H_2$]malate** (µmols/g)
Tumor		5.23 ± 0.63	0.08 ± 0.02	6.82 ± 0.84	1.81 ± 0.53
Kidney		11.03 ± 1.01	0.58 ± 0.03	7.20 ± 0.82	1.27 ± 0.39
Liver		2.06 ± 0.25	n.d.	2.14 ± 0.52	n.d.
Muscle		0.017 ± 0.011	n.d.	0.050 ± 0.016	n.d.
Heart					
0	18.80±0.50				
20 min	20.48±0.69	1.17±0.25	0.27±0.18		
60 min	21,21±0.78	0.87±0.024	0.31±0.09		
		Concentrations of protonated species			
Tumor		**Fumarate** (µmols/g)	**Malate** (µmols/g)	**Fumarate** (µmols/g)	**Malate** (µmols/g)
		6.92±2.65	0.75±0.44	7.72±1.72	3.74±0.21

Table 1 : Deuterium-labeled fumarate, malate and water concentrations measured in tissue extracts using ^2H NMR. The concentrations of the protonated species in tumors were measure, using ^1H NMR. For malate this was based on the upfield ^2H and ^1H resonances at 2.4 ppm since the downfield resonance was not resolved from the water resonance. The concentrations were measured in the indicated tissues 20 minutes after i.v. injection of [2,3-$^2H_2$]fumarate. The measurements in tumor, kidney, liver and skeletal muscle were made in EL4 tumor-bearing mice, which were either etoposide (67 mg/kg) or vehicle-treated (Control). The measurements in heart muscle were made in non-tumor bearing mice and extracts were made before (0) and at the indicated times after [2,3-$^2H_2$]fumarate injection. Data are expressed as the mean ± S.E.M. (n=3).

Metabolite	Concentration at specified time points following injection of [2,3-$^2H_2$]fumarate (mM)			
	20 min		70 min	
	BT	AT	BT	AT
[2,3-$^2H_2$]fumarate	12.35±3.61	10.08±0.89	4.95±1.43	4.45±0.50
[2,3-$^2H_2$]malate	0.03±0.01	0.47±0.05	0.004±0.003	0.19±0.09
HDO	20.16±1.14	19.32±1.68	22.68±1.42	23.52±1.21

Table 2: Deuterium-labeled fumarate and malate concentrations in the blood of EL4 tumor-bearing mice before (BT) and after (AT) etoposide-treatment. Blood was collected by cardiac puncture at the specified times after i.v. injection of 1 g/kg [2,3-$^2H_2$]fumarate and the concentrations measured using ^2H NMR. Data are expressed as mean ± S.E.M. (n=3).

Time after [2,3-$^2H_2$]fumarate addition (min)	[2,3-$^2H_2$]fumarate [mM]	[2,3-$^2H_2$]malate [mM]	HDO [mM]
5	7.45 ± 0.39	0.04 ± 0.03	11.73 ± 0.28
60	5.35 ± 0.89	0.25 ± 0.05	11.91 ± 0.50

Table 3: Deuterium-labeled fumarate, malate and water concentrations measured in mouse erythrocyte suspensions using ^2H NMR. The concentrations were measured at the indicated time points after the addition of 8 mM [2,3-$^2H_2$]fumarate. Data are expressed as mean ± S.E.M. (n=3).

Figure legends

Figure 1: (**A-D**) ^{2}H NMR spectra of murine lymphoma (EL4) cell culture medium. (**A**) Medium from untreated cells and (**B**) cells treated for 24 h with 15 μM etoposide, 1 minute after the addition of 5 mM [2,3-$^{2}H_2$]fumarate. (**C**) Medium from untreated cells and (**D**) cells treated for 24 h with etoposide, 2 h after the addition of [2,3-$^{2}H_2$]fumarate. (**E-F**) Deuterated fumarate, malate and water concentrations in medium from untreated (**E**) and etoposide-treated cells at the indicated times after addition of 5 mM [2,3-$^{2}H_2$]fumarate (**F**). Rate of malate production in untreated and etoposide-treated EL4 cell suspensions (***P*=0.0018) (±SD, n=3 biological replicates) (**G**). (**H-M**) Production of labeled malate and water in cultures of human colorectal (Colo205) and breast cancer (MDA-MB-231) cells following the addition of 5 mM [2,3-$^{2}H_2$]fumarate. Deuterated fumarate, malate and water concentrations in medium from untreated (**H,K**) and cells treated for 24 h with MEDI3039 (**I,L**), at the indicated times after the addition of 5 mM [2,3-$^{2}H_2$]fumarate. (**J,M**) Rate of labeled malate production in untreated and MEDI3039-treated Colo205 (****P*=0.008) (**J**) and MDA-MB-231 (*****P*<0.0001) cells (Data are presented as mean ±SD, n=3 biological replicates) (**M**).

Figure 2: ^{2}H MR spectroscopic measurements of labeled fumarate, malate and water concentrations in EL4 (**A - E**), MDA-MB-231 (**F - J**) and Colo205 (**K - O**) tumors. Tumor spectra were acquired before and 48 h after etoposide treatment (67 mg/kg) of EL4 tumor-bearing mice (n=3,***P* < 0.01, *****P* <0.0001 and before and 24 h after treatment of MDA-MB-231 (n=5, **P* < 0.05, ***P* < 0.01, ****P* <0.001) and Colo205 tumor-bearing mice (n=5, ****P* <0.001, *****P* <0.0001) with MEDI3039 (0.8 mg/kg). (**B, D, G, I, L, N**). Sum of 12 ^{2}H spectra recorded over 60 minutes. The [2,3-

$^{2}H_2$] fumarate injection (1 g/kg) started 5 min after the start of acquisition of the first spectrum. The peaks were fitted individually using prior knowledge. (**E,J,O**) Estimated tumor malate concentrations pre- and post-treatment at indicated time points after [2,3-$^{2}H_2$] fumarate injection. (*P < 0.05, **P < 0.01, ***P <0.001, ****P <0.0001). Data are shown as mean ± SD.

Figure 3: Malate/fumarate and malate/water signal ratios in EL4, MDA-MB-231 and Colo205 tumors before and after treatment. (**A**) Tumor [2,3-$^{2}H_2$]malate/[2,3-$^{2}H_2$]fumarate and (**B**) [2,3-$^{2}H_2$]malate/semi heavy water (HDO) ratios, obtained by summing the fumarate, malate and HOD signals over 65 minutes after injection of [2,3-$^{2}H_2$]fumarate, before treatment and at 48 hours after treatment of EL4 tumor-bearing mice with etoposide (67 mg/kg) (n=3, *P < 0.05, **P < 0.01). Data are presented as mean ± SD. (**C**) [2,3-$^{2}H_2$]malate/[2,3-$^{2}H_2$]fumarate and (**D**) [2,3-$^{2}H_2$]malate/semi heavy water (HDO) ratios before and at 24 h after treatment of MDA-MB-231 tumor-bearing mice with MEDI3039 (0.8 mg/kg) (n=5, **P < 0.01). (**E**) [2,3-$^{2}H_2$]malate/[2,3-$^{2}H_2$]fumarate ratio and (**F**) [2,3-$^{2}H_2$]malate/semi heavy water (HDO) ratios before and at 24 h after treatment of Colo205 tumor-bearing mice with MEDI3039 (0.8 mg/kg) (n=5, **P < 0.01, *** P <0.001). Data are shown as box and whisker plots.

Figure 4*:* Fumarase activity in the EL4, Colo205 and MDA-MB-231 cells (**A**) and tumors (**B**) following treatment with the indicated drug concentrations. Western blot analysis of fumarase expression in EL4 (**C**), Colo205 (**D**) and MDA-MB-231 (**E**) tumors following treatment with the indicated drug concentrations. Densitometric analysis of the western blots. Fumarase band intensities relative to those of GAPDH

(three biological replicates, data are presented as mean ± S.E.M., *P < 0.05, **P < 0.01, ***P < 0.001).

Figure 5: Volumes of (**A**) EL4, (**B**) MDA-MB-231 and (**C**) Colo205 tumors before and 48 h after etoposide treatment (EL4) or 24 h after MEDI3039 treatment (MDA-MB-231, Colo205) (n=5, data are presented as mean ± SD, ****P < 0.0001) **D)** ATP concentrations measured in tumor extracts before (n=5) and after (n=5) treatment, data are presented as mean ± SD, **P < 0.01, ***P < 0.001.

Figure 6: Histological assessment of tumor cell death following treatment. Tumor sections were stained for CC3 and TUNEL (n=5 per group, drug- and vehicle-treated.) CC3 (**A,B**) and TUNEL (**D,E**) staining of EL4 tumor sections taken 48 h after treatment of the animals with etoposide or drug vehicle (control). CC3 (**G,H,M,N**) and TUNEL (**J,K,P,Q**) staining of MDA-MB-231 and Colo205 tumor sections taken 24 hours after treatment of the animals with MEDI3039 (0.8 mg/kg) or drug vehicle (control). ****P < 0.0001.

F**igure 7:** Metabolite concentration maps in the central slice derived from dynamic 3D CSI images summed over the first 30 minutes of signal acquisition following [2,3-$^{2}H_2$]fumarate injection into EL4 tumor-bearing mice. The color code represents concentration (in mM) derived from the ratios of the peak intensities in the malate and fumarate maps to peak intensities in an initial HDO map and corrected for the number of ^{2}H labels per molecule and signal saturation. (**A-D**) The locations of the tumors are outlined by dotted white lines. Approximate concentration maps of (**A**)

fumarate pre-treatment; (**B**) malate pre-treatment; (**C**) fumarate 48 h post-treatment; (**D**) malate 48 h post-treatment.

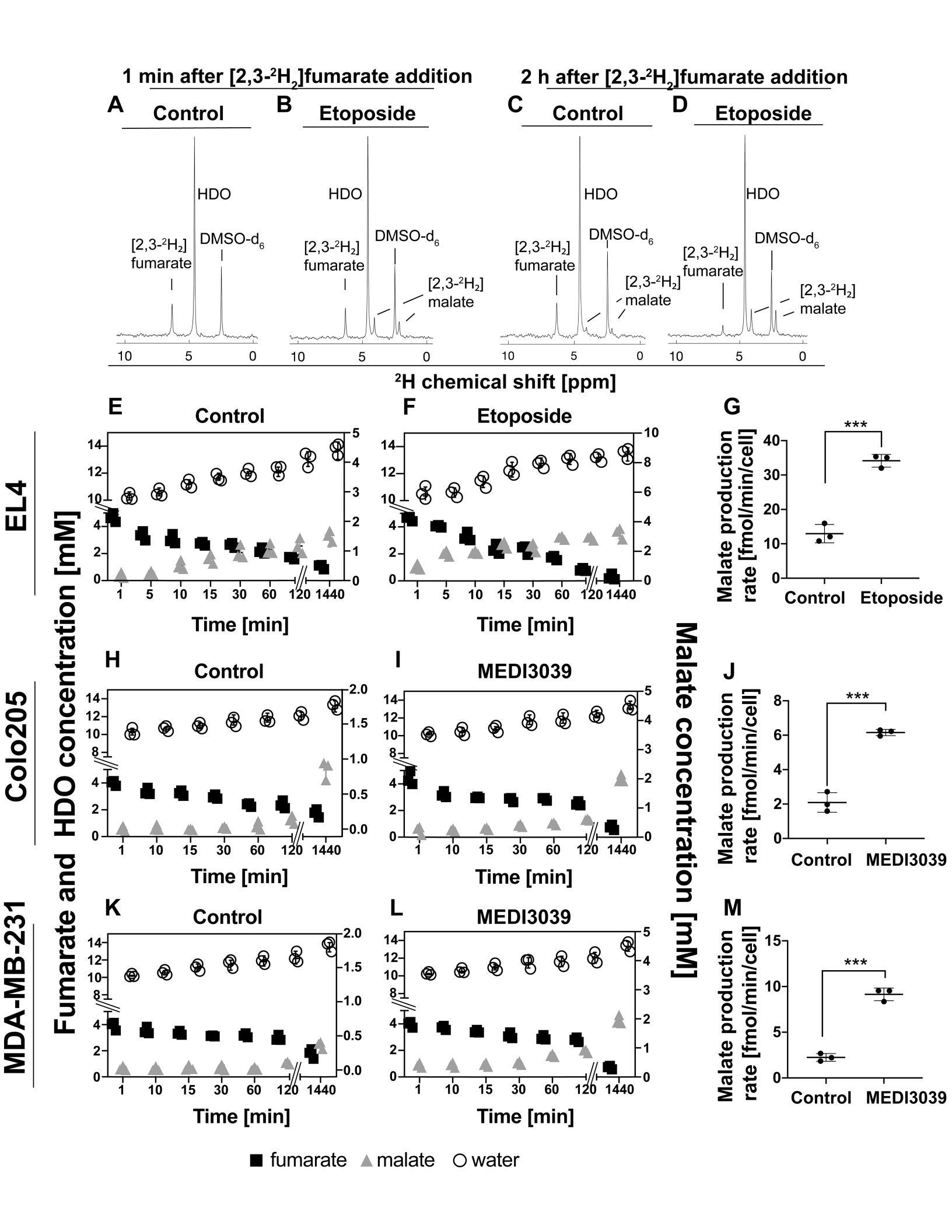
1 min after [2,3-²H₂]fumarate addition
2 h after [2,3-²H₂]fumarate addition
A Control
B Etoposide
C Control
D Etoposide
HDO
DMSO-d6
[2,3-²H₂] fumarate
[2,3-²H₂] malate
²H chemical shift [ppm]
EL4
Colo205
MDA-MB-231
E Control
F Etoposide
G
H Control
I MEDI3039
J
K Control
L MEDI3039
M
Time [min]
Fumarate and HDO concentration [mM]
Malate concentration [mM]
Malate production rate [fmol/min/cell]
Control
Etoposide
MEDI3039
***
fumarate
malate
water

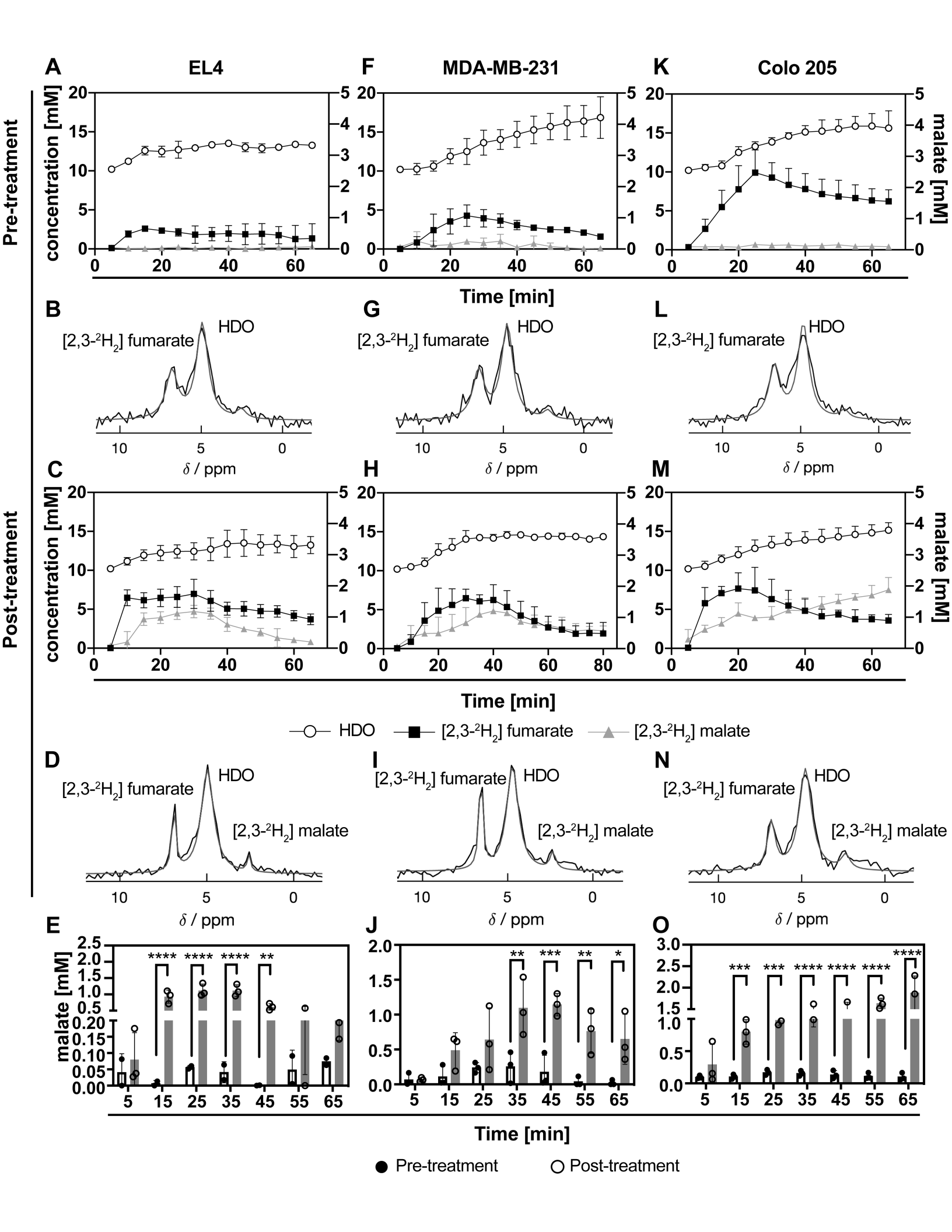
A
EL4
F
MDA-MB-231
K
Colo 205
Pre-treatment
Post-treatment
concentration [mM]
malate [mM]
Time [min]
B
G
L
HDO
[2,3-²H₂] fumarate
δ / ppm
C
H
M
D
I
N
[2,3-²H₂] malate
HDO
[2,3-²H₂] malate
[2,3-²H₂] fumarate
E
J
O
malate [mM]
Time [min]
Pre-treatment
Post-treatment

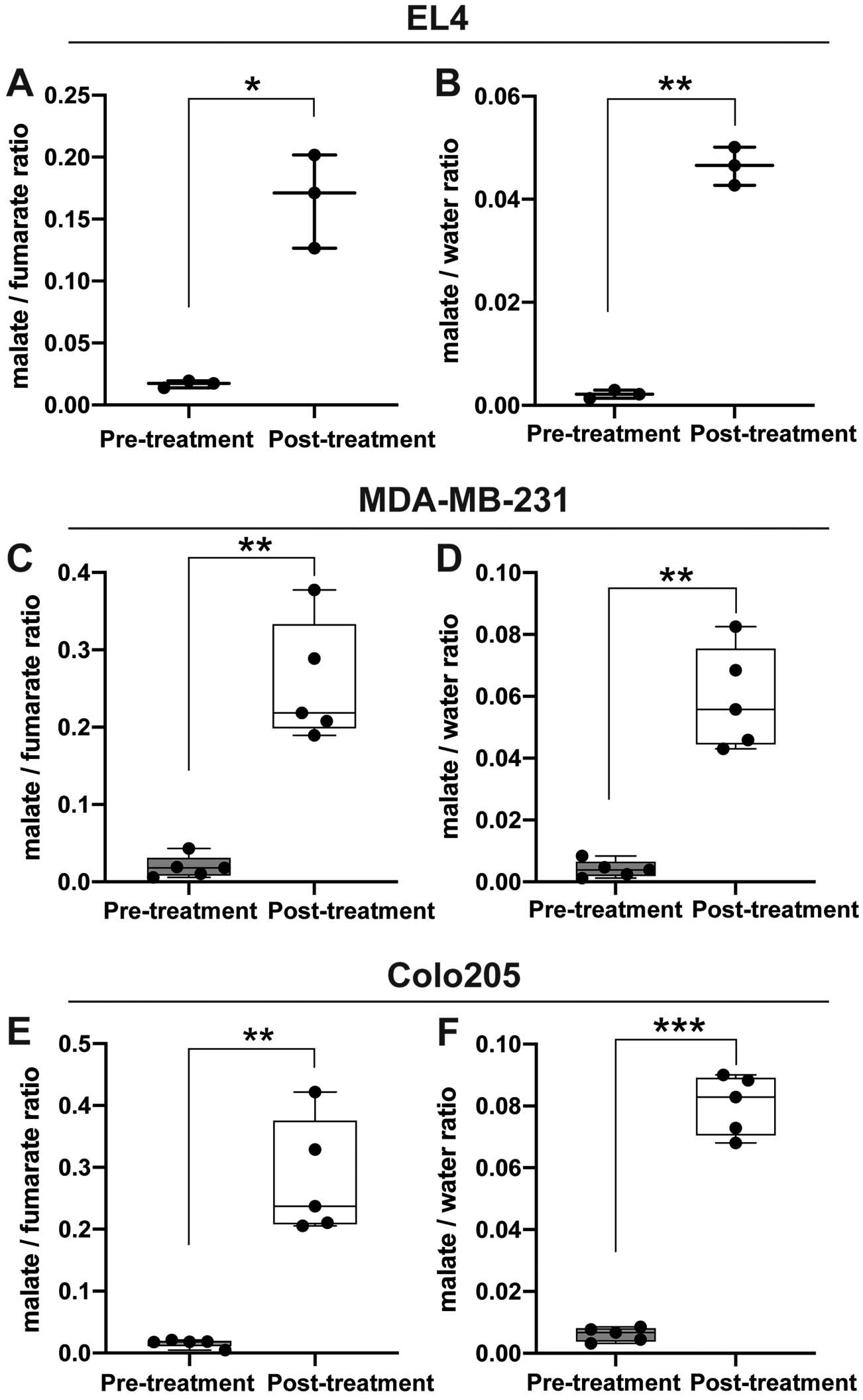
EL4
A
malate / fumarate ratio
0.25
0.20
0.15
0.10
0.05
0.00
*
Pre-treatment
Post-treatment
B
malate / water ratio
0.06
0.04
0.02
0.00
**
Pre-treatment
Post-treatment
MDA-MB-231
C
malate / fumarate ratio
0.4
0.3
0.2
0.1
0.0
**
Pre-treatment
Post-treatment
D
malate / water ratio
0.10
0.08
0.06
0.04
0.02
0.00
**
Pre-treatment
Post-treatment
Colo205
E
malate / fumarate ratio
0.5
0.4
0.3
0.2
0.1
0.0
**
Pre-treatment
Post-treatment
F
malate / water ratio
0.10
0.08
0.06
0.04
0.02
0.00
***
Pre-treatment
Post-treatment

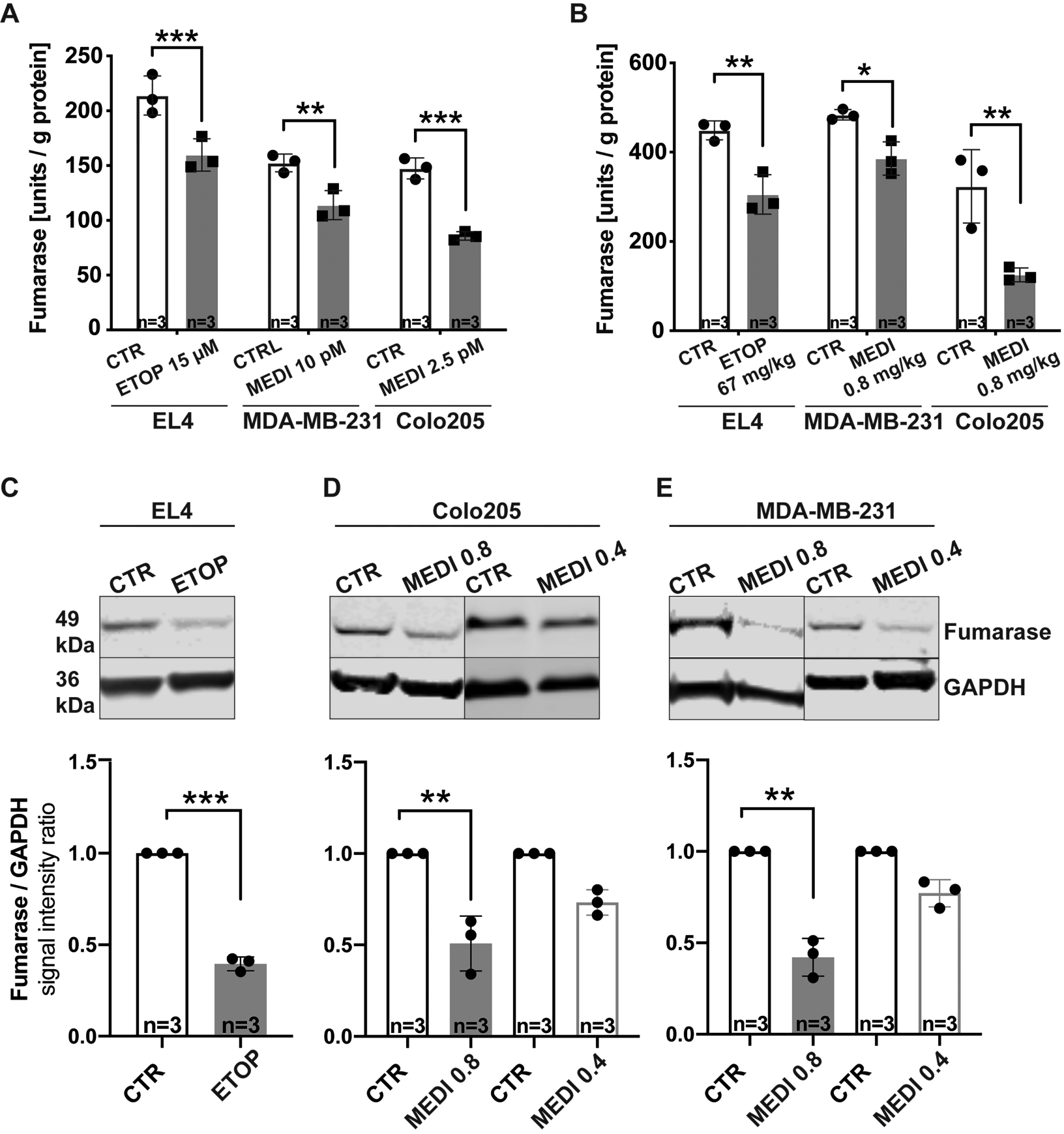
A
Fumarase [units / g protein]
250
200
150
100
50
0
***
**
***
n=3
n=3
n=3
n=3
n=3
n=3
CTR
ETOP 15 µM
CTRL
MEDI 10 pM
CTR
MEDI 2.5 pM
EL4
MDA-MB-231
Colo205
B
Fumarase [units / g protein]
600
400
200
0
**
*
**
n=3
n=3
n=3
n=3
n=3
n=3
CTR
ETOP 67 mg/kg
CTR
MEDI 0.8 mg/kg
CTR
MEDI 0.8 mg/kg
EL4
MDA-MB-231
Colo205
C
EL4
CTR
ETOP
49 kDa
36 kDa
Fumarase / GAPDH signal intensity ratio
1.5
1.0
0.5
0.0
***
n=3
n=3
CTR
ETOP
D
Colo205
CTR
MEDI 0.8
CTR
MEDI 0.4
**
n=3
n=3
n=3
n=3
CTR
MEDI 0.8
CTR
MEDI 0.4
E
MDA-MB-231
CTR
MEDI 0.8
CTR
MEDI 0.4
Fumarase
GAPDH
**
n=3
n=3
n=3
n=3
CTR
MEDI 0.8
CTR
MEDI 0.4

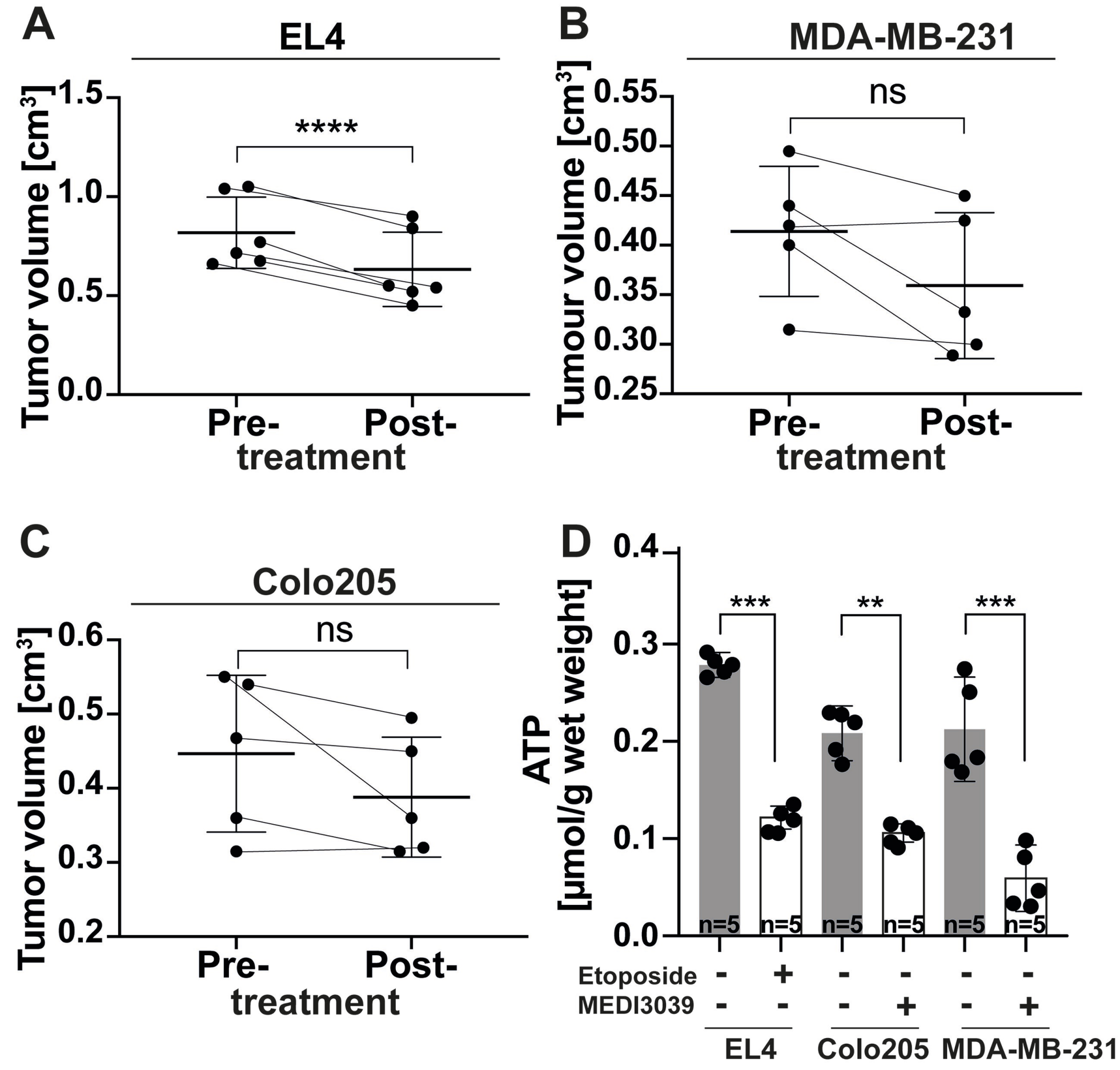
A
EL4
Tumor volume [cm³]
1.5
1.0
0.5
0.0
****
Pre-
treatment
Post-
B
MDA-MB-231
Tumour volume [cm³]
0.55
0.50
0.45
0.40
0.35
0.30
0.25
ns
Pre-
treatment
Post-
C
Colo205
Tumor volume [cm³]
0.6
0.5
0.4
0.3
0.2
ns
Pre-
treatment
Post-
D
ATP
[µmol/g wet weight]
0.4
0.3
0.2
0.1
0.0
***
**
***
n=5
n=5
n=5
n=5
n=5
n=5
Etoposide - + - - - -
MEDI3039 - - - + - +
EL4
Colo205
MDA-MB-231

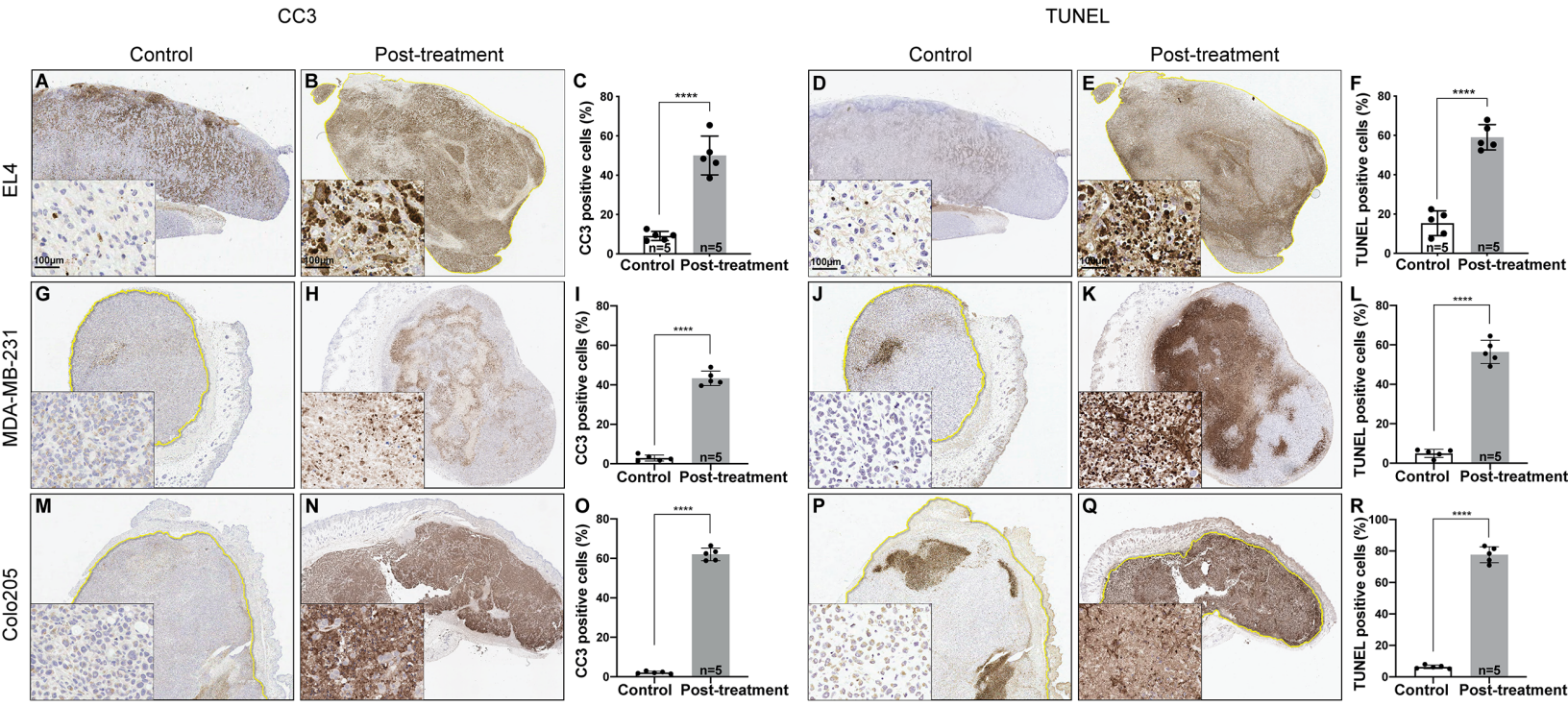
CC3
TUNEL
Control
Post-treatment
Control
Post-treatment
EL4
MDA-MB-231
Colo205
A
B
C
D
E
F
G
H
I
J
K
L
M
N
O
P
Q
R
100μm
CC3 positive cells (%)
TUNEL positive cells (%)
****
n=5
Control
Post-treatment

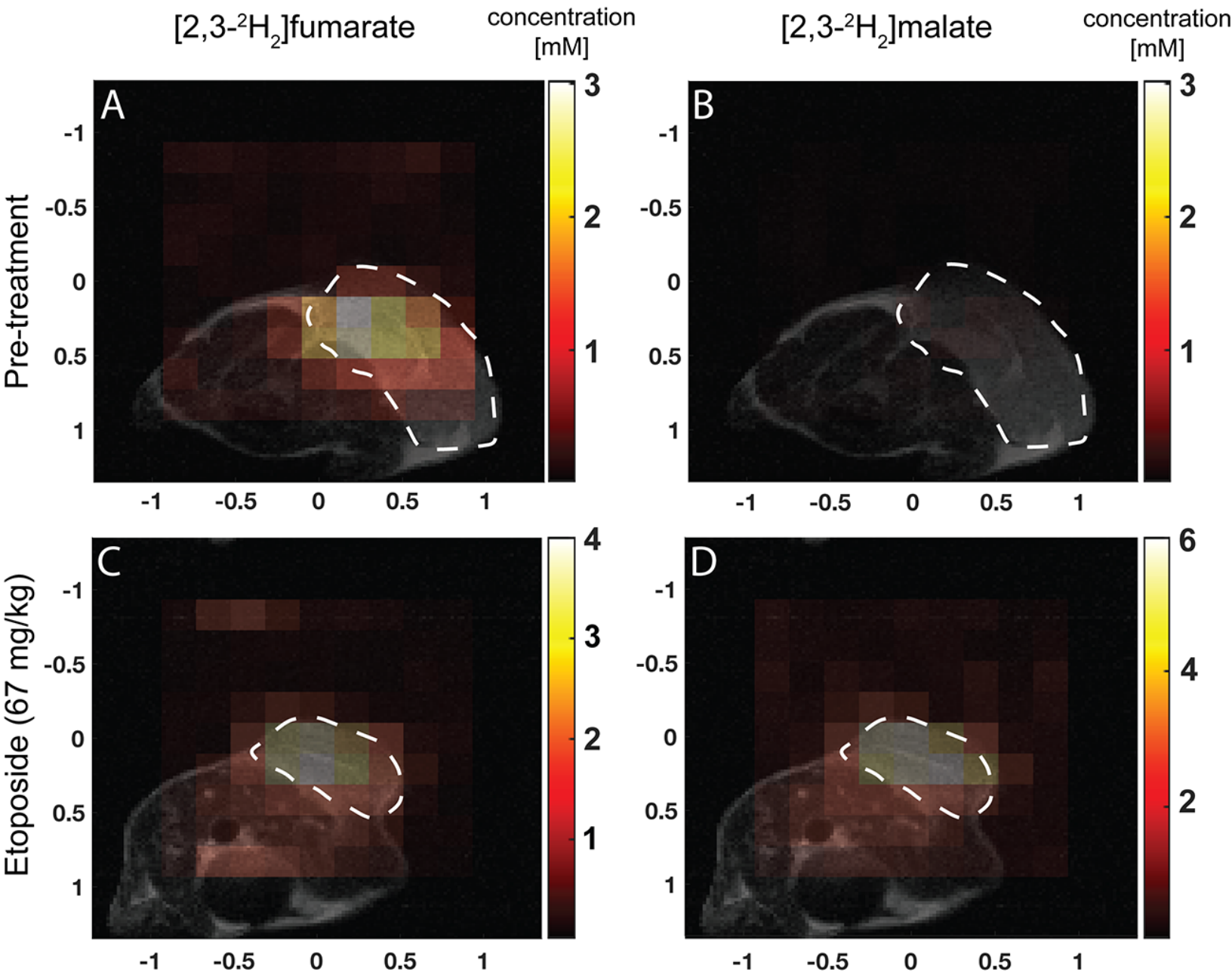
[2,3-$^2H_2$]fumarate
concentration [mM]
[2,3-$^2H_2$]malate
concentration [mM]
Pre-treatment
Etoposide (67 mg/kg)
A
B
C
D
-1
-0.5
0
0.5
1
3
2
1
4
6